Journal of Power Sources 307 (2016) 231–243

Contents lists available at ScienceDirect

Journal of Power Sources

journal homepage: www.elsevier.com/locate/jpowsour

Natural abundance ^{17}O, ^{6}Li NMR and molecular modeling studies of the solvation structures of lithium bis(fluorosulfonyl)imide/1,2-dimethoxyethane liquid electrolytes

Chuan Wan [a, b], Mary Y. Hu [a], Oleg Borodin [c], Jiangfeng Qian [a], Zhaohai Qin [b], Ji-Guang Zhang [a], Jian Zhi Hu [a, *]

[a] The Joint Center for Energy Storage Research (JCESR), Pacific Northwest National Laboratory, Richland, WA 99354, USA
[b] College of Science, China Agricultural University, Beijing 100193, China
[c] Electrochemistry Branch, Sensor & Electron Devices Directorate, US. Army Research Laboratory, Adelphi, MD 20783, USA

HIGHLIGHTS

- Natural abundance ^{17}O and ^{6}Li NMR spectra are acquired.
- Solvation structures are explored by combining NMR results with DFT and MD simulations.
- The Li^+ ion is fully separated by three DME molecules at dilute concentration.
- The coordination between Li^+ and FSI^- ion increases with increasing concentration.

GRAPHICAL ABSTRACT

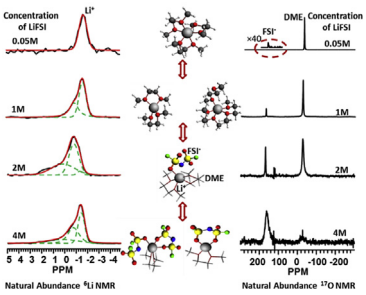

ARTICLE INFO

Article history:
Received 21 September 2015
Received in revised form
4 December 2015
Accepted 23 December 2015
Available online xxx

Keywords:
Natural abundance ^{17}O and ^{6}Li NMR
Molecular modeling studies
Electrolytes
Lithium bis(fluorosulfonyl)imide
1,2-Dimethoxyethane
Solvation structure

ABSTRACT

Natural abundance ^{17}O and ^{6}Li NMR experiments, quantum chemistry and molecular dynamics studies were employed to investigate the solvation structures of Li^+ at various concentrations of LiFSI in DME electrolytes. It was found that the chemical shifts of both ^{17}O and ^{6}Li changed with the concentration of LiFSI, indicating the changes of solvation structures with concentration. For the quantum chemistry calculations, the coordinated cluster $LiFSI(DME)_2$ forms at first, and its relative ratio increases with increasing LiFSI concentration to 1 M. Then the solvation structure LiFSI(DME) become the dominant component. As a result, the coordination of forming contact ion pairs between Li^+ and FSI^- ion increases, but the association between Li^+ and DME molecule decreases. Furthermore, at LiFSI concentration of 4 M the solvation structures associated with $Li^+(FSI^-)_2(DME)$, $Li^+_2(FSI^-)(DME)_4$ and $(LiFSI)_2(DME)_3$ become the dominant components. For the molecular dynamics simulation, with increasing concentration, the association between DME and Li^+ decreases, and the coordinated number of FSI^- increases, which is in perfect accord with the DFT results.

1. Introduction

Lithium-ion batteries (LIBs) is one of the most efficient electrochemical energy storage systems and has been widely used in

* Corresponding author.
E-mail address: Jianzhi.Hu@pnnl.gov (J.Z. Hu).

http://dx.doi.org/10.1016/j.jpowsour.2015.12.120
0378-7753/

portable electronic devices, electric vehicles (EVs) and grid energy storage. However, the limited energy density of the state of the art LIB using graphite anode still cannot meet the demands of high energy density applications such as long range EVs. Li metal is an ideal anode material because of its excellent physical and electrochemical properties: the low density (0.534 g cm^{-3}), the lowest negative electrochemical potential (−3.040 V vs. standard hydrogen electrode) and the highest theoretical energy density (3860 mAh g^{-1}). But the application of Li metal anode in rechargeable batteries is hindered by several challenges, including dendrite grown and low Columbic efficiency (CE) during the charging/discharging processes. After unsuccessful effort to use Li metal as an anode in rechargeable LIB in 1970s–1980s [1,2], graphite has been adopted as the predominate anode material for LIBs.

Electrolyte, a vital element of electrochemical batteries, is responsible for transferring Li^+ ion between the anode and the cathode. Because Li metal is thermodynamically unstable, the electrolyte molecule can react with Li metal anode, which can lead to the consumption of both the electrolyte and Li metal anode. Therefore, the electrochemical properties (including viscosity, ion conductivity etc.) of electrolyte play a critical role on the stability of Li metal anode and strongly affect the CE, cycle life and reliability of a battery [3–5]. As a result, designing an electrolyte with favorable molecular interaction between solvent molecules and Li^+ ions is one of the decisive factors for enhancing cell performance and stability. Studying Li^+ solvation structures in an electrolyte is thus important for understanding the fundamentals behind the cycling performance of a Li metal anode [6–9].

Glymes ($CH_3O(CH_2CH_2O)_nCH_3$, n = 1–4 for monoglyme to tetraglyme, respectively), containing two or more ether oxygen (Oe), provide high donor numbers and relatively strong Lewis basicity [10]. These aprotic saturated polyether solvents possess exceptional alkali metal salts solubility, leading to high ionic conductivity when used as electrolytes. Most of the literature reports revealed that electrolytes based on glyme solvents generally had a good property of inhibiting the growth of Li dendrite, but poor Li cycling efficiencies due to the formation of the oxidation degradation manifested by the covered lithium alkoxy species (ROLi) at the electrode interface, i.e., the solid electrolyte interface (SEI) [5,11,12]. Recently, significant efforts have been made to overcome the problem of poor Li cycling efficiencies [7,12,13]. In particular, Yamada and coworkers [14–16] reported the application of superconcentrated electrolytes in lithium ion batteries. At lower concentration, i.e., 1 M lithium bis(fluorosulfonyl)imide (LiFSI) in glyme solvent (1,2-dimethoxyethane (DME or monoglyme)), its reduction stability against graphite anode is poor due to the co-intercalation of Li^+ and solvent to destroy the layered structure of graphite. At higher concentration, i.e., 3.6 M electrolyte, the lithium intercalation into graphite anode is highly reversible, which can be ascribed to the sacrificed reduction of anions to form a stable SEI layer on anode. The oxidative stability of LiFSI in DME electrolyte at higher concentration is also enhanced as all the FSI^- anions and DME solvents will interact with Li^+ to form a polymeric complex, thus free DME solvents are eliminated. Furthermore, it has been reported recently by Qian and coworkers [17] that the high concentrated electrolyte consists of 4 M LiFSI in DME can limit dendrite growth and largely increase CE to more than 99% during Li cycling process by using lithium metal anode. Based on their initial analysis using the molecular dynamics (MD) simulations, nearly all of the ions were present as small to very large aggregate clusters in 4 M LiFSI/DME electrolyte. In contrast, more than half of the Li^+ cation and FSI^- anion were dissociated in a relatively low concentration electrolyte (1 M LiFSI/DME). The authors suggest that the highly coordinated FSI^- anions and solvents can reduce the electrolyte reductive ability; while the increased Li^+ concentration enables the high rate performance at the same time. High LiFSI salt aggregation in concentrated electrolytes also facilitated LiF formation upon electrolyte reduction [13]. However, the detailed changes in Li^+ solvation structures are not known at different LiFSI concentration in DME. It is therefore necessary to carry out further investigations to obtain in-depth understanding of the solvation environments of ions at various LiFSI concentrations in DME in order to further optimize the properties of electrolytes for practical applications of this electrolyte system.

NMR (nuclear magnetic resonance) spectroscopy, an atomic specific, non-destructive and inherently quantitative tool, has been used to elucidate the solvation structures and the ion coordination formulations of glyme electrolytes [8,18–24]. As early as in 1999, Hayashi et al. [25] employed ^7Li and ^{13}C NMR to investigate the Li^+ solvation state of DME/EC binary solvent electrolytes. Plewamarczewska et al. [8] have estimated the formation constants of XCF_3SO_3 (X = Li^+, Na^+, K^+ or n-Bu_4N^+) and $LiBF_4$ in glymes (monoglyme–triglyme) systems using a combination of ^7Li, ^{11}B and ^{19}F NMR. The experimental results from these prior studies showed that the ionic pair formation constant depends on the length of ether chain rather than the coordination states and dielectric properties. Yoshida et al. [7] reported an oxidative stable glyme (triglyme or tetraglyme)-lithium salt equimolar electrolytes, where ab initio molecular orbital calculations was used to demonstrate the donation of lone pairs of ether oxygen atoms to the Li^+ cation, and ^1H NMR was used to estimate the lifetime of the free glyme in equimolar complex, providing evidence to support the mechanism of ligand exchange conduction. ^{17}O NMR has emerged as a very sensitive probe for studying the interaction between an oxygen atom and a Li^+ cation due to its large chemical shift range [24]. However, ^{17}O NMR remains difficult because its low sensitivity arising from the rather low natural abundance (0.037%), and the usually broadline feature in spectrum as it is quadrupolar. Likewise, ^6Li NMR can be very useful for directly studying the solvation structures of Li^+ with the solvent molecules. But ^6Li also suffers from low sensitivity due to its low natural abundance of 7.42% and rather long spin-lattice relaxation time [24].

In this paper, natural abundance ^{17}O and ^6Li NMR were employed to study the solvation structures of LiFSI in DME based on the changes in chemical shift and linewidth at ultrahigh magnetic field of 20 T. To obtain a clearer physical picture on the interaction formations between Li^+ ions and DME as well as FSI^- anions, density functional theory (DFT) and MD simulations of the multinuclear NMR chemical shifts were employed to accurately assign the experimental results and related the experimental observations to the detailed molecular interaction to Li^+ solvation environment. These analyses demonstrate clearly how the coordination between salt ions and solvent molecules affect the electrochemical properties of Li deposition.

2. Experimental

2.1. Materials and sample preparations

1,2-dimethoxyethane (DME) was obtained from BASF Corporation. Lithium bis(fluorosulfonyl)imide (LiFSI) was obtained from Nippon Shokubai Co., Ltd. and used as received. A variety of electrolytes were prepared by dissolving the desired amount of LiFSI into the solvent DME. The conductivity results of 1 M to saturate electrolytes are shown in Table S1. The electrical conductivities of LiFSI in DME electrolytes decrease with the increase of electrolyte concentrations. The materials were stored and handled in an MBraun LABmaster glove box with an Argon atmosphere (<1 ppm O_2 and <1 ppm H_2O).

2.2. NMR measurements

All the natural abundance ^{17}O and ^{6}Li NMR experiments were performed on the Varian-Inova 850 MHz NMR spectrometer equipped with a homemade 15 mm outer diameter large-sample-volume probe, operating at a magnetic field of 19.975 T. The ^{17}O MAS spectra were acquired at 122.041 MHz using a single $\pi/4$ pulse with a pulse width of 30 μs with a recycle delay at 0.5 s. The ^{6}Li MAS spectra were acquired at 125.050 MHz using a single $\pi/4$ pulse with a pulse width of 20 μs with a recycle delay at 120 s ^{17}O and ^{6}Li chemical shifts were referenced to the water (H_2O, 0 ppm) and 1 M LiCl aqueous solution (0 ppm), respectively. All the NMR measurements were carried out at room temperature, i.e., 20 °C. The magnetic field and samples stability were confirmed (see Fig. S1). Spectral deconvolution was carried out by fitting lorentzian functions to the experimental spectra using the NUTs program (v.2012, Acorn NMR Inc., Las Positas, CA, USA).

2.3. Quantum chemistry calculations

The *Amsterdam Density Functional* (ADF-2014) package was used to run the computational modeling. The geometry optimization was carried out using the generalized gradient approximation (GGA) based Becke–Lee–Yang–Parr function with dispersion correction (BLYP-D) [26]. Furthermore, the QZ4P basis set (quad Z, 4 polarization function, all-electron) with the Slater type functional [27] was used to carry out all the calculations. For the calculation of NMR parameters, the geometry optimized structures at the same level of the theory and with the same basis set were used to evaluate the chemical shielding for each atom.

2.4. Molecular dynamics simulations methodology

Molecular dynamics (MD) simulations were performed at 333 K for four salt concentrations of (DME)LiFSI mixtures ranging from 9 DME per LiFSI to 1.4 DME per LiFSI. Compositions of MD simulation cells are shown in Table S2. Simulated electrolytes were created by replicating $(DME)_9LiFSI$ and $(DME)_7(LiFSI)_5$ clusters, resulting in a simulation box of 80 Å followed by equilibration NPT runs at 393 K for 5–7 ns. Initial configurations of $(DME)_{3.5}LiFSI$ and $(DME)_{2.33}$-LiFSI systems were created by removing LiFSI salt from equilibrated configurations of $(DME)_7(LiFSI)_5$ (DME:Li = 1.4) and equilibrating for 6 ns at 393 K. After that simulation temperature was dropped to 333 K and MD simulations were performed in NPT ensemble at P = 1 atm for durations shown in Table S2. These runs were not included in the analysis and considered to be equilibration runs. Production runs were performed at 333 K in the NVT ensemble using the average simulation box size from NPT ensemble for.

A many-body polarizable force field (FF) APPLE&P [28] (Atomistic Polarizable Potential for Liquids, Electrolytes, and Polymers) has been used. It utilizes an exp-6 form for description of non-bonded interactions in conjunction with permanent charges situated on atomic sites and off atomic sites for the FSI^- anion. The many-body polarization interactions are represented by the induced isotropic atomic dipoles. The short-range interaction between induced dipoles is screened using Thole methodology with the Thole parameter ($a_T = 0.2$). Atoms connected by bonds (1–2) and bends (1-2-3) were excluded from the list of non-bonded interactions. Atoms connected by 3 or more bonds had full non-bonded interactions with the exception that 1–4 interaction between permanent charges and induced dipoles were scaled by 0.8. Non-bonded interactions were cutoff at 12 Å. The following Ewald parameters were used k = 7 and $\alpha = 0.23$. A detailed discussion of the functional form and simulation parameters is provided elsewhere [28,29]. The LiFSI force field was largely taken from our recent work on (AN)LiFSI electrolytes and ionic liquids with the exception of the FSI^- oxygen polarizability that was reduced to 1.0 $Å^3$ in order to better reproduce binding energies of LiFSI obtained from quantum chemistry calculations [30]. DME force field parameters were taken from our previous work [17].

3. Results and discussions

3.1. ^{17}O and ^{6}Li NMR experimental results

Fig. 1 shows the natural abundance ^{17}O and ^{6}Li NMR spectra of LiFSI in DME at various LiFSI concentrations. The chemical shift values, linewidth, including the relative ratios of the various simulated peaks in ^{6}Li spectra, are summarized in Table 1, Tables S3 and S4. For Fig. 1a of ^{17}O spectra, in general, narrow ^{17}O peaks are obtained at low LiFSI concentration of 0.05 M and then gradually broadened with increasing of LiFSI concentration. the peaks at around 160 ppm can be assigned to the sulfonyl oxygen atoms (Os) of FSI^-, while the −23.9 ppm is attributed to the ethereal oxygen atoms (Oe) in pure DME. The chemical shifts of the Oe decrease (shifted upfield) monotonically with the increasing of LiFSI concentration, indicating that the coordinated DME molecules are increased with the increasing concentration of Li^+. The changes of chemical shifts of Os with LiFSI concentration is, however, more complicated. From 0.05 M to 2 M concentration, the chemical shifts of Os are increased with LiFSI concentration, reaching a maxima at about 2 M concentration, and then decreased with further increase of LiFSI concentration, i.e., from 3 M to saturated concentration. Therefore, the ion–dipole interaction between Li^+ ion and the Os of FSI^- ion, the common reason leading to an upfield shift, is the dominant mechanism responsible the decreased chemical shifts of Os with increasing LiFSI concentration at high LiFSI concentrations. At dilute concentrations, the increased chemical shifts with LiFSI concentration, however, cannot be explained by this simple model (see Fig. 2).

Fig. 1b shows the ^{6}Li NMR spectra of LiFSI/DME solutions. The ^{6}Li peaks are broadened from 0.05 M to 3 M concentration and then sharp narrowed at 4 M concentration and finally broadened at saturate concentration, indicating the quantity of Li^+ cluster spices decreased at the 4 M concentration. At low LiFSI concentration of 0.05 M, a single peak at −1.7 ppm is observed that is symmetric. The 0.5 M spectrum becomes asymmetric. Indeed, it can be fit well using two peaks with a major peak center at about −1.6 ppm and a minor peak at about −0.8 ppm. At 1 M concentration, the relative ratio of the −0.8 ppm peak is increased significantly. At 2 M concentration, the −1.6 ppm peak becomes almost invisible and the −0.8 ppm peak becomes the dominant peak. At this concentration, a third broad peak centered at about 0.2 ppm is clearly observed. Upon further increase the LiFSI concentration to 3 M, the relative ratio of the 0.2 ppm peak is increased. However, at 4 M LiFSI concentration, the peak is sharply narrowed, indicating some peculiar behavior is observed, the major peak is upfield shifted to −0.7 ppm when compared with the results obtained on the 3 M case of −0.6 ppm. The changes of both chemical shifts and relative ratios of various peaks obviously reflect the changes of the Li^+ ion solvation structure at various LiFSI concentrations. In the following, quantum chemistry calculations on a series of possible model solvation structures and the molecular dynamics modeling of various LiFSI/DME concentrations are used for interpreting the changes associated with the observed NMR parameters and for identifying the most probable solvation structures at different concentration of LiFSI in DME.

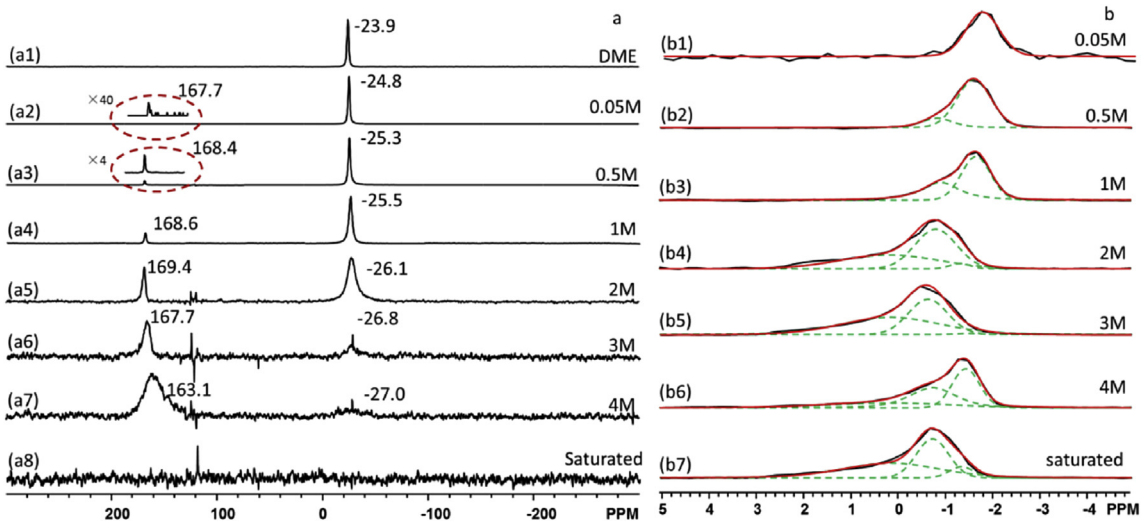

Fig. 1. (a): Natural abundance ^{17}O NMR spectra LiFSI/DME electrolytes at different LiFSI concentrations acquired using a recycle delay time of 0.5 s: (a1) The solvent DME, with 464 scans; (a2) 0.05 M solution, with 89,812 scans; (a3) 0.5 M solution, with 20,588 scans; (a4) 1 M solution, with 9468 scans; (a5) 2 M solution, with 10,560 scans; (a6) 3 M solution, with 11,644 scans; (a7) 4 M solution, with 15,508 scans; (a8) Saturated solution, with 116,448 scans. The line broadening used for processing the data was 50 Hz. (b): Natural abundance ^{6}Li NMR spectra of LiFSI/DME electrolytes at various LiFSI concentrations acquired using a recycle delay time of 120 s: (b1) 0.05 M solution, with 512 scans; (b2) 0.5 M solution, with 512 scans; (b3) 1 M solution, with 64 scans; (b4) 2 M solution, with 42 scans, (b5) 3 M solution, with 512 scans; (b6) 4 M solution, with 14 scans; (b7) Saturated solution, with 16 scans. The line broadening used for processing the data was 20 Hz.

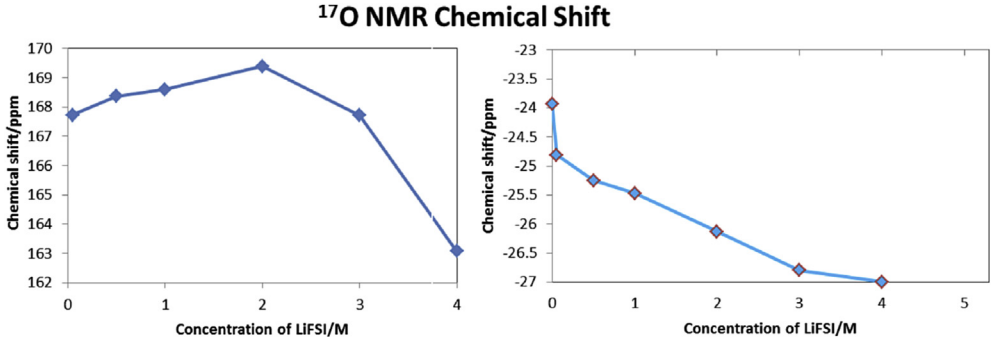

Fig. 2. Experimentally obtained ^{17}O chemical shifts of various LiFSI concentrations (0 M–4 M) according to Table 1.

Table 1
The experimentally obtained ^{17}O and ^{6}Li NMR chemical shifts at different LIFSI concentrations in DME.

Concentration	DME/LiFSI molar ratio[a]	^{17}O chemical shift		^{6}Li spectra simulation chemical shift		
0 M (pure DME)		–	−23.9	–		
0.05 M	192.4	167.7	−24.8	–	–	−1.7
0.5 M	19.2	168.4	−25.3	–	−0.8	−1.6
1 M	9.6	168.6	−25.5	–	−0.9	−1.6
2 M	4.8	169.4	−26.1	0.2	−0.8	−1.3
3 M	3.2	167.7	−26.8	0.2	−0.6	−1.4
4 M	2.4	163.1	−27.0	0.2	−0.7	−1.4
Saturate (5.3 M)	1.8	–	–	0.2	−0.7	−1.3

[a] The relative molar ratio of DME molecules when the concentration of LiFSI is normalized to 1 M.

3.2. DFT computational modeling of ^{17}O and ^{6}Li NMR chemical shift

3.2.1. Selecting chemical shift reference

DMSO was used as the ^{17}O chemical shift reference by adding 252 ppm to the calculated absolute shift, as was reported by Deng et al. [24] $Li^{+}(H_2O)_4$ was used as the ^{6}Li chemical shift reference by adding 87.9 ppm to the calculated absolute shift [31].

3.2.2. Predicting ^{17}O chemical shift in neat DME

The ^{17}O chemical shifts of gas phase DME were calculated first. The calculated result of −30.9 ppm on an isolated molecule does not match well with the experimental value of −23.9 ppm. Since inter molecular interaction inevitably exists in DME solution, calculations on DME dimer, trimer, hexamer and 12 DME cluster were carried out. The chemical shifts of calculated results are summarized in Table S5. Obviously, with the increase of the DME cluster size, the calculated values are gradually approaching the experimental values. This gives us confidence that quantum chemistry calculations can be used for predicting chemical shift values in electrolytes.

3.2.3. Predicting ^{17}O and ^{6}Li chemical shift on model clusters containing one or two Li^{+} cation interacting with DME molecules: a case valid for low concentration of LiFSI in DME

Based on phase diagram studies of LiTFSI, $LiMF_6$ (M = Sb, As or P) and LiX (X = I or Br) Henderson et al. [32] suggested that the salvation shell structures of these Li salt/glyme solutions are primarily affected by the concentration. One Li^{+} ion can fully solvates with 3 glyme molecules at dilute concentration. At this solvent-separated

ion pairs (SSIP) situation, the Li^+ ion is coordinated by all of the 6 ether oxygen atoms. However, the detail solvation structure of LiFSI in DME has not yet been studied. Stimulated by the work of Henderson et al. discussed above, geometry optimization and NMR calculations were performed on clusters where one or two Li^+ ions are placed in the core, and the first solvation shells are constructed by 1–5 DME molecules, respectively, in order to gain insights into the solvation structure of LiFSI in DME at low concentration of LiFSI. Under this condition, the Li^+ and FSI^- are completely separated to form their own solvation structures. These simplified solvation structures are valid only at low concentrations such as 0.05 M and 0.5 M LiFSI. Five forms of oxygen coordination, including 2, 3, 4, 5 and 6-coordinated, are summarized in Table 2 and Fig. 3. For 2 oxygen coordination, the only one that is energetically stable is $Li^+(DME)_1$ (Table 2b). For 3 oxygen coordination, there are two possible structures. The first structure is $Li^+(DME)_2$ (Table 2c), where the Li^+ is coordinated with both oxygen in one DME molecule and the third oxygen in the second DME molecule. The second structure is $Li^+{}_2(DME)_3$ (Table 2d) as depicted in Fig. 3d, where one DME molecule is sandwiched between the two Li^+ ions. Similarly, the details of the coordination for the 4, 5 and 6 are summarized in Fig. 3 and Table 2. The quantum chemistry predicted ^6Li and ^{17}O chemical shifts on the various structures are also summarized in Table 2.

It is clear from Table 2 that in general, Li^+ with lower number of oxygen coordination, i.e., 2, 3 and 4-coordinate, exhibits higher ^6Li chemical shift values than those with higher coordinated number (i.e., 5 and 6-coordinate). In particular, for the case of 6-coordinate of $Li^+(DME)_3$ cluster, the predicted ^6Li chemical shift value of −1.3 ppm is already close to the experimental value of −1.7 ppm that is obtained from the sample of 0.05 M LiFSI in DME. Such nice agreement between experiment and theory indicates that at dilute concentration of LiFSI in DME, Li^+ and FSI^- are dissociated and the first shell solvation structure of a Li^+ contains 3 DME molecules, where the Li^+ is coordinated by all the six oxygen from the three DME molecules. The effects of second solvation shells to the ^6Li chemical shift values are further investigated on first solvation shell models labeled by "f" for $Li^+(DME)_2$ and "l" for $Li^+(DME)_3$ in Fig. 3 and Table 2. The reason for choosing these two basic models is that the first solvation shell structures are stable during full geometry optimization process as all the oxygen atoms from the first shell DME molecules are coordinated with the Li^+. Adding a second solvation shell containing 2, 4, 6 or 8 additional DME molecules have a strong impact on the ^6Li chemical shifts as is clearly shown by the quantum chemistry predicted ^6Li chemical shifts in Table 2. For example, for the 4-coordinate core $Li^+(DME)_2$, with the increase of second shell molecule, the ^6Li chemical shift moves upfield and reaches −0.9 ppm for the case of $Li^+(DME)_2(DME)_6$ (Table 2i), where the second solvation shell contains 6 DME molecules. Further increase the number of DME in the second solvation shell did not generate a stable structure (i.e., never converges). The −0.9 ppm chemical shifts is still far away from the experimentally observed −1.7 ppm for the dilute LiFSI in DME, i.e., 0.05 M case. Therefore, we can rule out the possibility of this solvation structure in dilute solution. In contrast, for the 6-coordinate core $Li^+(DME)_3$, with the increasing number of second shell molecules, the ^6Li chemical shift value moves downfield first (i.e., the value becomes less negative) for the cases containing 2, 4 and 6 DME in the 2nd solvation shell. The value of ^6Li chemical shift, however, jumps to −1.5 ppm for the case of $Li^+(DME)_3(DME)_8$, the largest 2nd solvation shell that is energetically stable. Since −1.5 ppm is in excellent agreement with the experiment value −1.7 ppm, the solvation structure of $Li^+(DME)_3(DME)_8$ is thus identified as the most likely Li^+ solvation structure at dilute LiFSI concentration in DME based on experimental ^6Li NMR data and quantum chemistry calculations. To further confirm the solvation structure of $Li^+(DME)_3(DME)_8$ at dilute LiFSI concentration in DME, ^{17}O results are evaluated below. Under the condition of dilute solution, i.e. ≤1 M, in general, the solvent DME molecules in the solvation shells (including both the first and second shells) are undergoing fast molecular exchange with the DME molecules in the bulk phase (<1.0 ns) [33], which is similar to the previously predicted Li-DME residence times (~4 ns) for DME-LiTFSI [34]. Under the condition of fast molecular exchange the experimentally observed ^{17}O chemical

Table 2
Quantum chemistry predicted ^{17}O chemical shifts on various Li^+ solvation structures in DME where Li^+ and FSI^- are fully dissociated.

Li^+ coordination #	System		^{17}O averaged predicted chemical shift[a, b]	Weight averaged ^{17}O chemical shift for Various concentrations[c]			^6Li averaged predicted chemical shift
				0.05 M	0.5 M	1 M	
	#	Experimental chemical shift	–	−24.8	−25.3	−25.5	
2-coordinate	b	$Li^+(DME)_1$	−27.4	−23.9	−24.0	−24.0	−0.4
3-coordinate	c	$Li^+(DME)_2$	−26.7	−23.9	−24.2	−24.5	0.3
	d	$Li^+{}_2(DME)_3$	−28.7	−24.0	−24.3	−24.7	0.2
4-coordinate	e	$Li^+(DME)_4$	−24.6	−23.9	−24.1	−24.2	−0.2
	f	$Li^+(DME)_2$	−27.4	−23.9	−24.3	−24.7	0.0
	g	$Li^+(DME)_2(DME)_2$	−29.2	−24.0	−25.0	−26.1	−0.2
	h	$Li^+(DME)_2(DME)_4$	−26.6	−24.0	−24.8	−25.6	−0.9
	i	$Li^+(DME)_2(DME)_6$	−29.5	−24.2	−26.2	−28.5	−0.9
5-coordinate	j	$Li^+(DME)_3$	−30.6	−24.0	−25.0	−26.0	−0.9
	k	$Li^+{}_2(DME)_5$	−31.6	−24.0	−24.9	−25.9	−0.7
6-coordinate	l	$Li^+(DME)_3$	−32.5	−24.0	−25.3	−26.6	−1.3
	m	$Li^+(DME)_3(DME)_2$	−31.0	−24.1	−25.8	−27.6	−1.3
	n	$Li^+(DME)_3(DME)_4$	−29.9	−24.1	−26.1	−28.3	−1.2
	o	$Li^+(DME)_3(DME)_6$	−30.5	−24.2	−27.0	−30.1	−1.1
	p	$Li^+(DME)_3(DME)_8$	−28.5	−24.2	−26.6	–	−1.5

[a] The ^{17}O chemical shifts are reported as the average of the shifts of all the oxygen in a model. This is valid because in solution due to fast and random molecular motion, one is unable to tell the difference between the various oxygen atoms that are bonded differently to Li^+ in a solvation structure.
[b] DMSO for ^{17}O and $Li^+(H_2O)_4$ for ^6Li were used as the chemical shift references for quantum chemistry calculations for converting the calculated results to the experimental scale.
[c] Weight averaged ^{17}O chemical shifts by considering the fast molecular exchange of the solvation shell DME molecules with the bulk DME molecules at dilute concentration, i.e. ≤1 M.

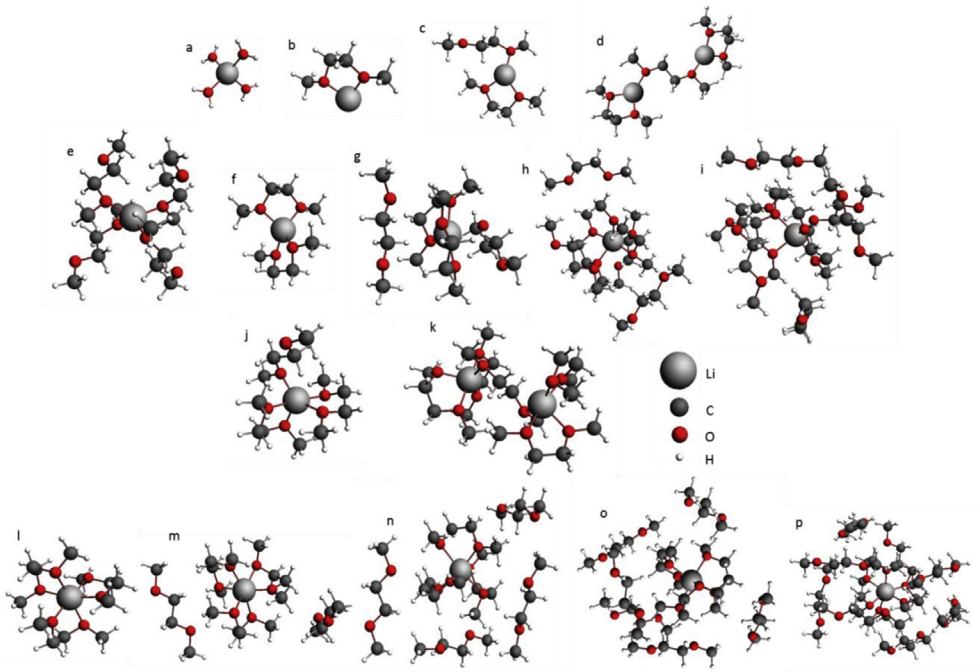

Fig. 3. Geometry optimized structures of Li^+ solvation structures. First row: (a) ^6Li reference standard of $Li^+(H_2O)_4$, where a Li^+ is bonded with $4H_2O$. (b) 2-coordinate $Li^+(DME)_1$, where a Li^+ is bonded with 1 DME. (c) $Li^+(DME)_2$, where a Li^+ is bonded with 2 DME by 3 Oxygen. (d) 3-coordinate $Li^+{}_2(DME)_3$, where 2 Li^+ are bonded with 2DME. Second row 4-coordinate: (e) $Li^+(DME)_4$, where a Li^+ is bonded with 4 DME by 4 Oxygen. (f) $Li^+(DME)_2$, where a Li^+ is bonded with 2 DME by 4 Oxygen. (g) $Li^+(DME)_2(DME)_2$, where 2 DME at first shell, 2 DME at second shell. (h) $Li^+(DME)_2(DME)_4$, where 2 DME at first shell, 4 DME at second shell. (i) $Li^+(DME)_2(DME)_6$, where 2 DME at first shell, 6 DME at second shell. Third row 5-coordinate: (j) $Li^+(DME)_3$, where a Li^+ is bonded with 3 DME by 5 Oxygen. (k) $Li^+{}_2(DME)_5$, where 2 Li^+ are bonded with 5 DME. Forth row 6-coordinate: (l) $Li^+(DME)_3$, where a Li^+ is bonded with 2 DME by 6 Oxygen. (m) $Li^+(DME)_3(DME)_2$, where 3 DME at first shell, 2 DME at second shell. (n) $Li^+(DME)_3(DME)_4$, where 3 DME at first shell, 4 DME at second shell. (o) $Li^+(DME)_3(DME)_6$, where 3 DME at first shell, 6 DME at second shell. (p) $Li^+(DME)_3(DME)_8$, where 3 DME at first shell, 8 DME at second shell.

shift is a single peak with peak center determined by the weighted averaged chemical shifts between the coordinated and the bulk DME molecules [6] in accordance with the following equation.

$$\delta_{average} = (a/(a+b)) \times \delta_A + (\ b/(a+b)) \times \delta_B \quad (1)$$

where δ_A is the experimentally observed ^{17}O chemical shift of bulk pure DME (−23.9 ppm), δ_B is the quantum chemistry predicted shift on a fixed solvation model, "a" is the molar ratio of DME molecules that are in the bulk DME solvent while "b" is the molar ratio of DME molecules that are in the solvation shells (including both the first and the second shells). The results are included in Table 2. For the 0.05 M LiFSI in DME, a ^{17}O chemical shift of −24.2 ppm is obtained for the solvation structure of $(Li^+(DME)_3(DME)_8$, which is in the excellent agreement with the experimental value of −24.8 ppm. This result strongly confirm the conclusion from ^6Li results that the solvation structure of $(Li^+(DME)_3(DME)_8$ is indeed the correct solvation structure of Li^+ in system of LiFSI/DME at such extremely dilute LiFSI concentration.

As already discussed earlier, at 0.5 M LiFSI in DME, the ^6Li spectrum can be simulated by two peaks with the major peak at −1.6 ppm and the minor shoulder peak at −0.8 ppm. For the −0.8 ppm peak, there are four possibilities based on the agreement between the predicted and the experimental ^{17}O of Oe in DME (−25.3 ppm) and ^6Li chemical shift values (see Tables 1 and 2). These four possibilities are two 4-coordinate structures: $Li^+(DME)_2(DME)_4$ (Table 2h, −0.9 ppm for ^6Li and −24.8 ppm for ^{17}O), $Li^+(DME)_2(DME)_6$ (Table 2i, −0.9 ppm for ^6Li and −26.2 ppm for ^{17}O) and two 5-coordinate structures: $Li^+(DME)_3$ (Table 2j, −0.9 ppm for ^6Li and −25.0 ppm for ^{17}O), $Li^+{}_2(DME)_5$ (Table 2k, −0.7 ppm for ^6Li and −24.9 ppm for ^{17}O). These relatively low coordinated clusters indicate that the coordinated number of Li^+/DME decrease with the increase concentration of LiFSI at the dilute condition.

3.2.4. The role of FSI^-

Firstly, the ^{17}O chemical shift on gas phase FSI^- anion was calculated. As shown in Table 3, the predicted ^{17}O chemical shift (190.4 ppm) of anion cannot match the experimental results (167.7 ppm) of 0.05 M LiFSI in DME, where LiFSI ion-pairs are fully separated [6,32,35]. Since the chemical shift of Os should be closed to that of isolated FSI^- anion, for the convenience of comparing the calculated ^{17}O chemical shifts on various solvation structures with the experimental results obtained at different LiFSI concentrations in DME, the theoretic ^{17}O chemical shift values of Os are re-referenced by subtracting 22.7 ppm from the predicted values.

Not like the monotonically decreased trend of ^{17}O chemical shift of the Oe oxygen in DME with the increasing concentration of LiFSI, the ^{17}O chemical shifts of the Os in FSI^- increases first with LiFSI concentration for LiFSI concentration below 2 M, reaching peak value at 2 M, and then decrease sharply from 3 M and beyond. As discussed above, in the case of extremely low concentration, the Li^+ and FSI^- are solvent-separated, where Li^+ is 6-coordinate in its first solvation shell as $Li^+(DME)_3$. In the following, we will use the $Li^+(DME)_3$ structure as the starting point to construct the FSI^- included complexes. Considering the case of 1:1 ratio of Li^+ cation to FSI^- anion in LiFSI, two kinds of DME replacement can be designed: (1) one of the DME molecule in $Li^+(DME)_3$ is replaced by one FSI^- to form $LiFSI(DME)_2$; (2) one of a DME's Li^+ bonded oxygen atom is replaced with one Os in FSI^- to obtain $LiFSI(DME)_3$. The resultant structures are summarized in Table S6 for the first replacement scheme and Table S7a for the second replacement scheme. For the $LiFSI(DME)_2$ structures in Table S6, $LiFSI(DME)_2$-1 has nitrogen atom directly coordinated with Li^+ with Li—N distance

Table 3
The calculated ^{17}O and ^{6}Li chemical shifts of LiFSI/DME solvation shell. DMSO and $Li^+(H_2O)_4$ were used as the reference for chemical shift standards.

#	System	^{17}O predicted chemical shift for FSI^-		^{17}O predicted chemical shift for DME	^{6}Li predicted chemical shift
		Average	Re-reference[a]	Average	Average
a	FSI^-	190.4	167.7	–	–
b	$LiFSI(DME)_2$-1	190.1	168.7	−27.8	−1.2
c	$LiFSI(DME)_2$-2	187.0	164.3	−26.5	−1.5
d	LiFSI(DME)-1	187.9	165.3	−28.5	−0.2
e	LiFSI(DME)-2	184.6	162.0	−27.4	0.2
f	$(LiFSI)_2(DME)_2$	191.9	169.2	−26.0	−1.0
g	$(LiFSI)_2(DME)_3$-1	191.8	169.1	−30.2	−1.0
h	$(LiFSI)_2(DME)_3$-2	189.3	166.6	−27.9	−0.9
i	$(LiFSI)_2(DME)_3$-3	184.9	162.3	−26.2	−1.1
j	$Li^+{}_2(FSI^-)(DME)_2$-1	191.5	168.8	−29.2	−0.7
k	$Li^+{}_2(FSI^-)(DME)_4$-1	189.2	166.6	−27.4	−1.2
l	$Li^+{}_2(FSI^-)(DME)_4$-2	186.9	164.3	−26.6	−1.0
m	$Li^+(FSI^-)_2(DME)$-1	184.5	164.8	−27.7	−1.6
n	$Li^+(FSI^-)_2(DME)$-2	187.2	164.5	−24.3	−1.1

[a] Re-reference the Os chemical shift of the 0.05 M LiFSI/DME to the experimental value of 167.7 ppm by subtracting 22.7 ppm from the predicted values for FSI^- in the Table.

of 2.3 Å. The bonding energy (−8.0303 Hartree) associated with this solvation structure is the lowest one among all the 4 possibilities, suggesting high probability of existence in the DME solution. The predicted ^{17}O chemical shifts for Os is the only value (168.7 ppm) that is higher than the experimental value of 168.6 ppm for LiFSI concentrations at 1 M. And the predicted ^{6}Li chemical shift (−1.2 ppm) of $LiFSI(DME)_2$-1 is also close to the most upfield ^{6}Li chemical shift at the concentration of 0.05 M–1 M (i.e., −1.6 ppm to −1.7 ppm), especially the upfield peak at the concentration of 2 M (−1.3 ppm). Furthermore, the structure of $LiFSI(DME)_2$-2, where the two Os in a FSI^- anion coordinate with the Li^+, has the 2nd low bonding energy (−8.0293 Hartree) that is very close to the value of 8.0303 Hartree associated with $LiFSI(DME)_2$-1, indicating the probability of the existence of this structure in the solution is close to that of $LiFSI(DME)_2$-1. Interestingly, the configuration of $LiFSI(DME)_2$-2 has a predicted ^{6}Li chemical shift of −1.5 ppm that is in an even better agreement with the experimental values of 0.05 M to 1 M (−1.6 ppm to −1.7 ppm), suggesting the co-existence of $LiFSI(DME)_2$-1 and $LiFSI(DME)_2$-2 in the 0.5 and 1 M solutions. Furthermore, the very low relative ^{6}Li peak area of −1.3 ppm peak at 2 M concentration (i.e., 3.3%, see Table S4) strongly indicates that the structures of $LiFSI(DME)_2$ are decreased (even vanished) at the concentration higher than 2 M. In contrast, the other two configurations, i.e., $LiFSI(DME)_2$-3 and $LiFSI(DME)_2$-4, in Table S6 have higher bonding energies (−8.0188 and −0.80136 Hartree), suggesting the probability of their existence is less than the first two possibilities at LiFSI concentrations of ≤2 M. However, the ^{17}O Os chemical shifts (165.4 and 166.1 ppm) and ^{6}Li chemical shifts (−1.0 and −0.8 ppm) of these two configurations can well match both the experimental results of ^{17}O (167.7 ppm for Os and −26.8 ppm for Oe) and ^{6}Li (−0.6 ppm) at 3 M LiFSI concentration, indicating the possibility of the existence of these configurations at 3 M. It is notable that, in the case of high LiFSI/DME concentrations, the weight averaged value can't accurately represent the actually change of the Oe chemical shift, because the slow exchange between the shell and bulk DME molecule at high viscosity and high coordination of high concentrations.

In contrast, for the second replacement method, i.e., the structure of $LiFSI(DME)_3$ in Table S7a, the ^{6}Li chemical shift value of −2.1 ppm is much lower than the experimental value of the most upfield ^{6}Li peak across the concentration studied, i.e., from 0.05 M to saturation LiFSI concentration in DME (−1.3 to −1.7 ppm), suggesting their existence in the solution is unlikely. Therefore, the slight increase of the ^{17}O chemical shifts of Os for LiFSI concentration below 1 M concentration is from the gradual increase of the 6-coordinate $Li^+(DME)_3$ that is replaced by one FSI^- anion. As a result, to assign the increase and then decrease trend of ^{17}O chemical shifts as well as the −0.8 ppm and −1.6 ppm ^{6}Li peak, the solvation structures of $LiFSI(DME)_2$-1 and $LiFSI(DME)_2$-2 are among the preferred FSI^- including solvation structures at LiFSI concentration below 2 M while the solvation structures of $LiFSI(DME)_2$-3 and $LiFSI(DME)_2$-4 are among the preferred structures at 3 M. To help with the discussion, the possible solvation structures at various LiFSI concentrations in DME are summarized in Schemes 1 and 2 along with the quantum chemistry predicted ^{17}O chemical shifts for Os and Oe, and ^{6}Li chemical shifts.

For concentration at 2 M and beyond, the configurations of $LiFSI(DME)_2$ along cannot explain the third deconvoluted broad ^{6}Li peak centered at about 0.2 ppm and the decrease of the Os chemical shifts from 169.4 ppm (2 M concentration) to 163.1 ppm (4 M concentration). It is known from Table 2 that the ^{6}Li chemical shifts of the fully dissociated complex 3-coordinate $Li^+(DME)_2$ (0.3 ppm) and $Li^+{}_2(DME)_3$ (0.2 ppm) are in excellent agreement with the experimental value of the 0.2 ppm for the most downfield ^{6}Li spectral peak in the experimental spectra (Fig. 1b and Scheme 2). A careful evaluation at the change of the relative peak area ratio of the 0.2 ppm ^{6}Li peak reveals some interesting behavior, i.e., an increase in the relative peak area of the 0.2 ppm peak from 2 M (44.0%) to 3 M (57.4%), followed by a decrease from 3 M (57.4%) to 4 M (24.9%) and finally an increase from 4 M (24.9%) to (48.4%) at saturation. Apparently, the 3-coordinate $Li^+(DME)_2$ (0.3 ppm) and $Li^+{}_2(DME)_3$ (0.2 ppm) along cannot explain such peculiar behavior. In order to explain the experimental trend of ^{6}Li NMR for LiFSI concentration above 2 M, the 3-coordinate $Li^+(DME)_2$ is used as the parent structure to form FSI^- included complexes where the one Oe coordinated DME molecule is replaced by one FSI^- anion. The reason for including FSI^- is due to the fact that at high LiFSI concentration, the incorporation of FSI^- into Li^+ solvation structures must happen. The resultant two possibilities of the complexes (LiFSI(DME)-1 and LiFSI(DME)-2) are given in both Fig. 4 and Table 3 (also see Schemes 1 and 2). The LiFSI(DME)-1 (Table 3d, where the Li^+ is coordinated by one Os) and LiFSI(DME)-2 (Table 3e, where the Li^+ is coordinated by two Os) have predicted ^{6}Li chemical shift values of −0.2 ppm and 0.2 ppm that are in agreement with the experimental ^{6}Li chemical shift of 0.2 ppm for LiFSI concentration ≥ 2 M (see Fig. 1b and Scheme 2). Furthermore, the predicted Os ^{17}O chemical shift values of 165.3 ppm for LiFSI(DME)-1 and 162.0 ppm for LiFSI(DME)-2 both are less than the predicted ^{17}O Os chemical shift value of

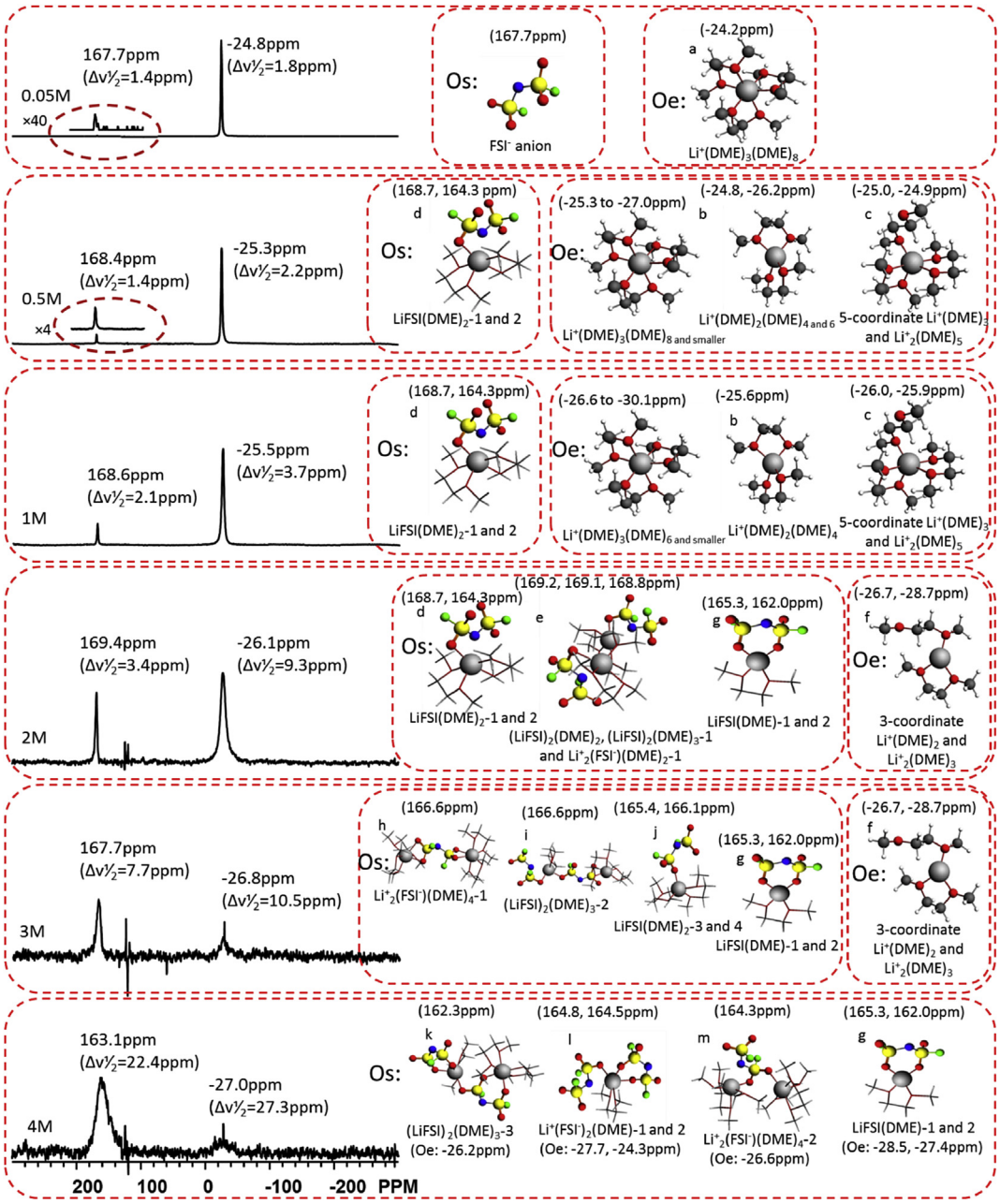

Scheme 1. The changes of solvation structures at various LiFSI concentration in DME for explaining the ^{17}O NMR spectra at different LiFSI concentrations Note that to simplify the labeling only the first solvation shells are listed here.

168.7 ppm for LiFSI(DME)$_2$-1, a trend that is in agreement with the experimentally observed ^{17}O Os chemical shifts with the increase of the LiFSI concentration, i.e., the trend of first increase and then decrease across the LiFSI concentration studied. Therefore, at concentrations of 2 M and 3 M the major component of the 0.2 ppm ^6Li peak is the 3-coordinate $Li^+(DME)_2$ and $Li^+{}_2(DME)_3$ solvation structures, and at high concentrations (i.e.,4 M and saturation) the major component of the 0.2 ppm ^6Li peak is due to the FSI^- including structures of LiFSI(DME). These results clearly demonstrate that the content of LiFSI in LiFSI/DME electrolytes can enormously impact the solvation structures. Furthermore, the investigating of the two highfield ^6Li NMR peaks i.e., the −0.6 to −0.8 ppm, and the −1.3 to −1.4 ppm for LiFSI concentration ≥2 M, including the discussion of structures of Table 3f–n and Table S7b–d, is located in Supplementary Materials, and all the experimental and calculated results are summarized in Scheme 1 (^{17}O) and Scheme 2 (^6Li) as well as Table 4. As a result, with the increase of LiFSI concentration, the association between Li^+ and DME molecule is decreased, and the coordination between Li^+ and FSI^- ion is increased.

As mention above, an irregular trend of the relative ^6Li peak area for the 0.2 ppm peak is observed at the saturated concentration. In this case, the ^{17}O spectrum is too broad to be detected at saturation concentration of LiFSI in DME due to the significantly decreased molecular motion. On the other hand, ^6Li NMR peaks are still observed. The relative peak area ratios of the three deconvoluted peaks in ^6Li spectrum are surprisingly changed where the downfield peaks (0.2 ppm and −0.7 ppm) change into the major ones and

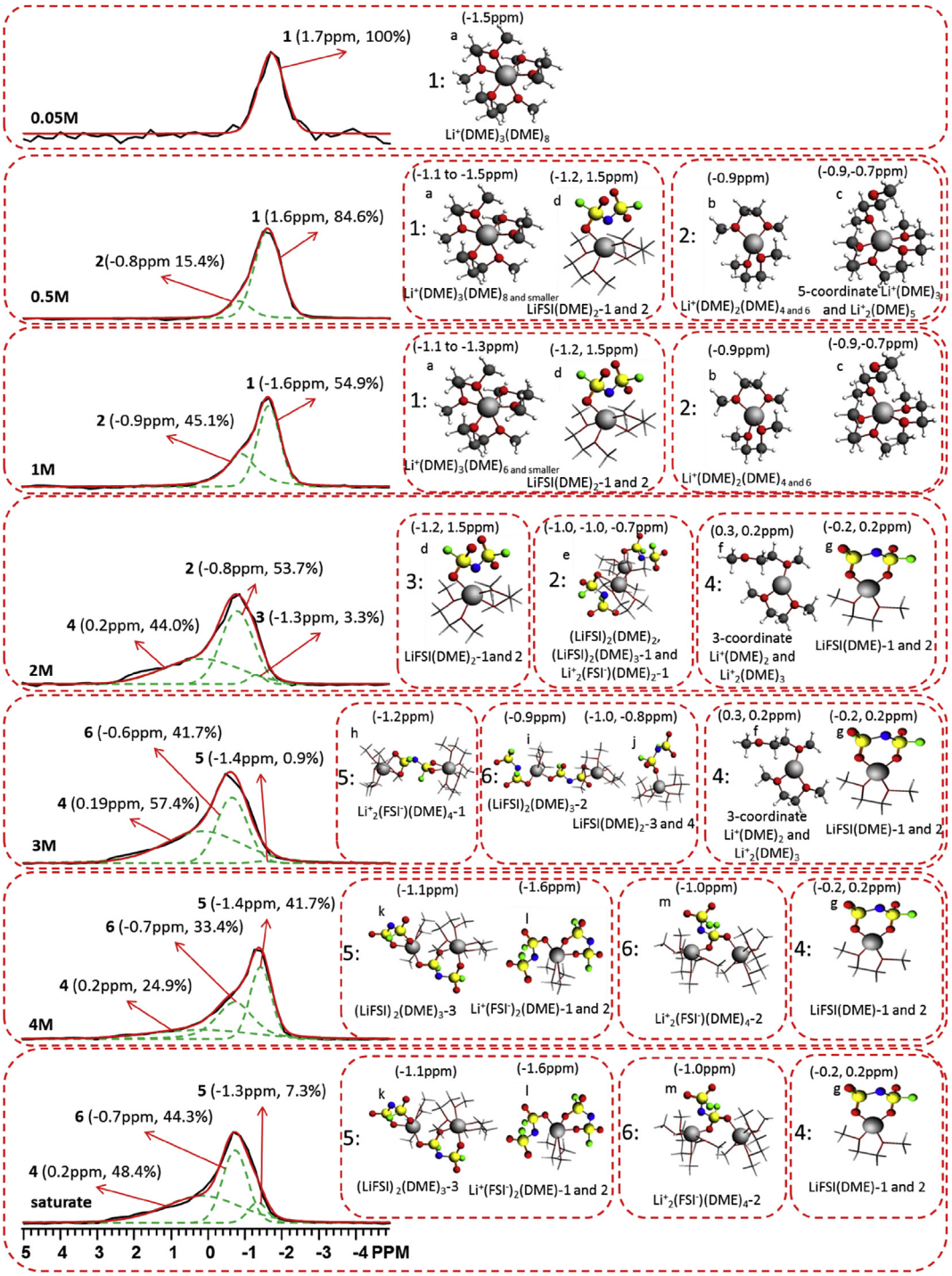

Scheme 2. The changes of solvation structures at various LiFSI concentration in DME for explaining the ^{6}Li NMR spectra at different LiFSI concentrations Note that to simplify the labeling only the first solvation shells are listed here.

the upfield peak (−1.3 ppm) becomes the minor one. Based on the similar ^{6}Li chemical shifts between the saturated and the 4 M samples, it is apparent that the basic solvation structures are the same between the 4 M and the saturated concentration samples, but the distribution of the various solvation structures are significantly different. For example, in the case of the 4 M sample, the solvation structures of $(LiFSI)_2(DME)_3$-3 (Table 3i), $Li^+(FSI^-)_2(DME)$-1 and 2 (Table 3m and n) and $Li^+_2(FSI^-)(DME)_4$ are the dominant structures while at saturation concentration the structures of LiFSI(DME)-1 and 2 (Table 3d and e) and $Li^+_2(FSI^-)(DME)_4$ are the dominant solvation structures (see Supplementary Materials). It has been reported that best electrical performance has been achieved with the 4 M concentration electrolytes in Li-metal battery [17]. The result strongly indicate that the solvation structures of $Li^+(FSI^-)_2(DME)$ are important structures that contribute to the best electrochemical performance reported previously.

As a conclusion, in order to accurately understand the

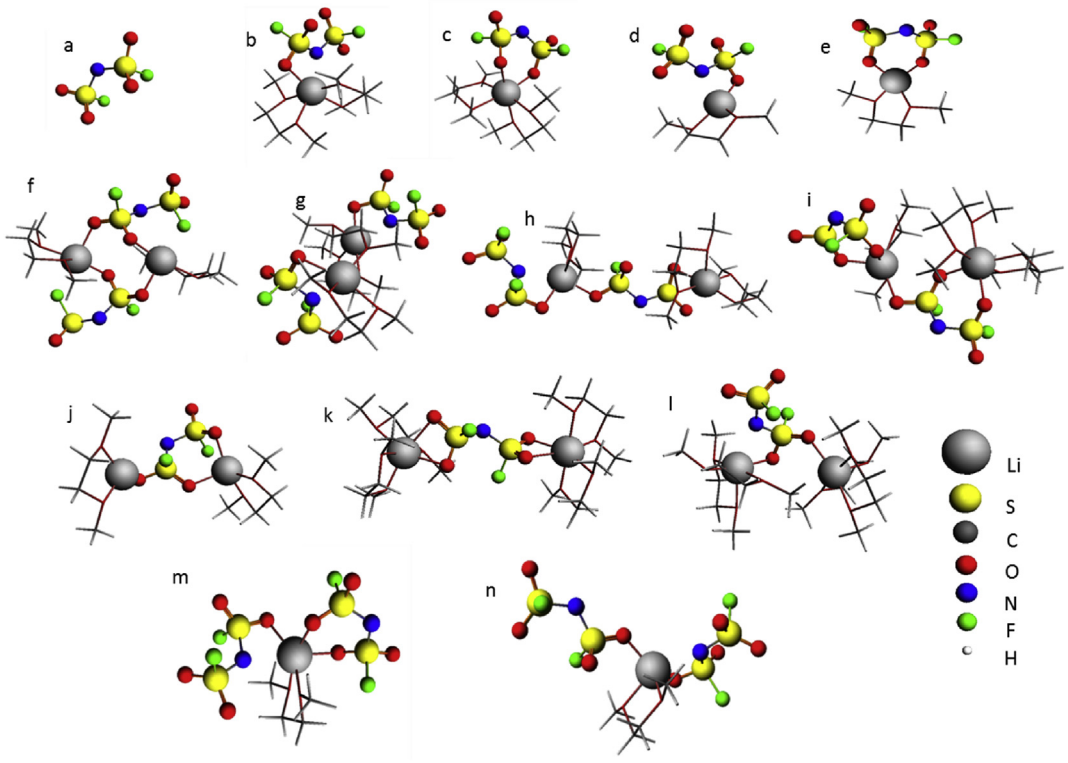

Fig. 4. Geometry optimized structures of Li^+ solvation shell by including FSI^-. a) FSI^- (gas phase). b) $LiFSI(DME)_2$-1, where a Li^+ ion is bonded by FSI^- ion via one Os and 2 DME. c) $LiFSI(DME)_2$-2, where a Li^+ ion is bonded by FSI^- ion via two Os and 2 DME. d) LiFSI(DME)-1, where a Li^+ ion is bonded by FSI^- ion via one Os and 1 DME. e) LiFSI(DME)-2, where a Li^+ ion is bonded by FSI^- ion via two Os and 1 DME. f) $(LiFSI)_2(DME)_2$, where two 3d structures linked together via the same S atoms by bonding to Os. g) $(LiFSI)_2(DME)_3$-1, where two 3d linked together via a DME molecule. h) $(LiFSI)_2(DME)_3$-2, where a 3b and a 3d structures linked together via the different S atoms by bonding to Os of 3b. i) $(LiFSI)_2(DME)_3$-3, where a 3c and a 3e structures linked together via the FSI^- ion of 3c. j) $Li^+{}_2(FSI^-)(DME)_2$-1, where two 2b linked together via the same S atom by bonding to Os of a FSI^- ion. k) $Li^+{}_2(FSI^-)(DME)_4$-1, where two 2f structures linked together via the different S atoms by boding to Os of a FSI^- ion. l) $Li^+{}_2(FSI^-)(DME)_4$-2, where two 2f structures linked together via the same S atom by boding to Os of a FSI^- ion. m) $Li^+(FSI^-)_2(DME)$-1, where a 3e after adding a FSI^-. n) $Li^+(FSI^-)_2(DME)$-2, where a 3d after adding a FSI^-.

Table 4
Possible predicted solvation structures for explaining the ^6Li NMR spectra.

Concentration	Position (ppm)	Ratio	Possible structures	
0.05 M	−1.7	100%	$Li^+(DME)_3(DME)_8$	
0.5 M	−0.8	15.4%	(4-coordinate) $Li^+(DME)_2(DME)_{4\text{ or }6}$	(5-coordinate) $Li^+(DME)_3$ or $Li^+{}_2(DME)_5$
	−1.6	84.6%	$Li^+(DME)_3(DME)_{8\text{ or smaller}}$	$LiFSI(DME)_2$-1 or 2
1 M	−0.9	45.1%	(4-coordinate) $Li^+(DME)_2(DME)_{4\text{ or }6}$	(5-coordinate) $Li^+(DME)_3$ or $Li^+{}_2(DME)_5$
	−1.6	54.9%	$Li^+(DME)_3(DME)_{6\text{ or smaller}}$	$LiFSI(DME)_2$-1 or 2
2 M	0.2	44.0%	(3-coordinate) $Li^+(DME)_2$ or $Li^+{}_2(DME)_3$	LiFSI(DME)-1 or 2
	−0.8	53.7%	$(LiFSI)_2(DME)_2$ $(LiFSI)_2(DME)_3$-1 $Li^+{}_2(FSI^-)(DME)_2$-1	(5-coordinate) $Li^+(DME)_3$ or $Li^+{}_2(DME)_5$
	−1.3	3.3%	$LiFSI(DME)_2$-1 or 2	
3 M	0.2	57.4%	(3-coordinate) $Li^+(DME)_2$ or $Li^+{}_2(DME)_3$	LiFSI(DME)-1 or 2
	−0.6	41.7%	$(LiFSI)_2(DME)_3$-2	$LiFSI(DME)_2$-3 or 4
	−1.4	0.9%	$Li^+{}_2(FSI^-)(DME)_4$-1	$Li^+(FSI^-)_2(DME)$-1 or 2
4 M	0.2	24.9%	LiFSI(DME)-1 or 2	
	−0.7	33.4%	$Li^+{}_2(FSI^-)(DME)_4$-2	
	−1.4	41.7%	$(LiFSI)_2(DME)_3$-3	$Li^+(FSI^-)_2(DME)$-1 or 2
Saturate	0.2	48.4%	LiFSI(DME)-1 or 2	
	−0.7	44.3%	$Li^+{}_2(FSI^-)(DME)_4$-2	
	−1.3	7.3%	$(LiFSI)_2(DME)_3$-3	$Li^+(FSI^-)_2(DME)$-1 or 2

experimental results, quantum chemistry calculations of the ^{17}O and ^6Li chemical shift were conducted on proposed solvation structures. It was found that at low LiFSI concentrations (<1 M), most of the Li^+ cation and FSI^- anion are fully dissociated. The first solvation shell of a Li^+ ion is coordinated with 3 DME molecules *via* bonding with 6 oxygen atoms. Addition of second solvation shells improves the agreement between experimental and computational results. The experimentally observed ^{17}O chemical shift is a weight average between bonded (including first and second solvation shells) and bulk DME molecules due to fast exchange between the coordinated DME molecules and bulk solvent DME molecules. For the FSI^- included structures, at relative high concentrations (i.e., from 0.5 M to 1 M), the complex of $LiFSI(DME)_2$ forms at first, and its ratio increases with the increase of LiFSI concentration. The fast

exchange between the bonded and the bulk FSI^- anion as well as the bulk solvent molecules again can explain the observed ^{17}O chemical shifts of the Os in FSI^-. The relatively low coordinated number of fully DME coordinated Li^+ (4 and 5-coordinate) are also observed at this case. At concentrations higher than 1 M, formation of LiFSI(DME) is evident. With the increase of LiFSI concentration, the coordinated number of Li^+/DME is decreased, and the coordination of forming contact ion pairs between Li^+ and FSI^- ion is increased, and the solvation structures associated with $Li^+(FSI^-)_2(DME)$, $(LiFSI)_2(DME)_3$,$Li^+_2(FSI^-)(DME)_4$ and LiFSI(DME) become the dominant components. It's supposed that the increased salt/solvent solvation structure minimized solvent decomposition during electrochemical deposition process, while decreased association between Li^+ and DME molecular facilitate the fast movement of Li^+ ions in high concentration LiFSI-DME electrolytes. The relationship between lithium ion transport number and lithium ion diffusion coefficient investigations with simulated structures at various concentrations would be great topics for the study of insight on the fundamental mechanism on these high efficient electrolytes.

4. Molecular dynamics simulations results

Radial distribution functions (RDFs) for the Li^+ cation with Oe of DME and with the FSI^- oxygen atoms were calculated and are shown in Fig. 5. The magnitude and position of the first peak of Li-Oe RDFs remains approximately constant with increasing salt concentration, thus indicating that the number of Oe in the Li^+ coordination shell will scale proportionally to the DME number density for all simulated salt concentrations. The magnitude of the first peak of Li-Os(FSI^-) RDF peak exhibits relatively slight decrease as salt concentration increases from 1 M to 2.3 M followed by a sharp increase with a subsequent salt concentration increase to 3.1 M and then 4.2 M. This behavior correlates well with the minimum and then sharp maximum of the Os chemical shifts observed in NMR measurements (see Fig. 1a). Nevertheless the magnitude of the first Li-Oe(DME) peak is 2–3 times higher than the Li-Os(FSI^-) peak indicating high propensity of Li^+ to coordinate with DME instead of FSI^-.

Next, we analyze changes of the composition of the Li^+ first coordination shell as a function of concentration. The size of the first Li^+ coordination shell was chosen as the average position of the first minimum of the Li-Oe(DME) and Li-Os(FSI^-) RDFs and set to 3.4 Å. Composition of the first Li^+ coordination shell is shown in Fig. 6. In the most dilute simulated salt concentration (1 M LiFSI concentration), a Li^+ cation is coordinated by 5.44 Oe of DME and 0.3 oxygens from the FSI^- anions. Essentially no fluorine atoms (less than 0.01) from the FSI^- anions were found in the Li^+ first

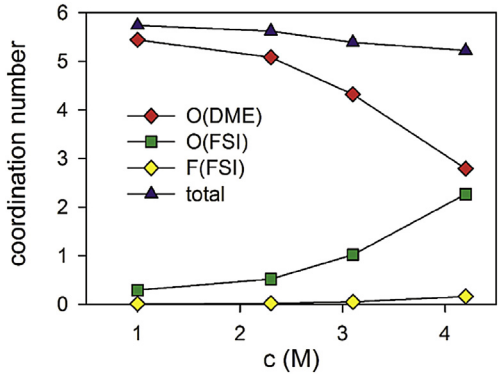

Fig. 6. Composition of the first Li^+ coordination shell (R < 3.4 Å) predicted from MD simulations.

coordination shell. This result is in accord with the discussions of Section 3.2.3, which suggest that the major coordinated clusters of Li^+ are $Li^+(DME)_3$ and $Li^+(DME)_2$ at the dilute LiFSI concentrations ($\leq$1 M). Addition of LiFSI salt up to 2.2 M results in a minor change in the composition of the Li^+ first coordination shell. At 1 M LiFSI salt concentration, most LiFSI exists as solvent separated ion pairs (SSIP) as the number of Os(FSI^-) in contract with Li^+ is significantly below one and reaches one only when salt concentration reaches 3.1 M. At 4.2 M there is a similar contribution from Oe(DME) and Os(FSI^-) to the Li^+ coordination. As discussed in Section 3.2.4, the majority of the Li^+ coordinated clusters are both FSI^- and DME included structures at $\geq$4 M LiFSI concentration, such as LiFSI(DME), $Li^+(FSI^-)_2(DME)$ and $(LiFSI)_2(DME)_3$. Therefore, the DFT computational results are consistent with the MD predictions at the high LiFSI concentrations. Previous quantum chemistry and experimental study reported reduction potential of DME-LiFSI to be around 1.6 and 2.3 V for the cases when the FSI^- anion was coordinated by one or two Li^+ in DME, respectively [13], indicating the importance of detailed understanding of SSIP and aggregate formation in DME-LiFSI for SEI formation at the negative electrode. In this study we find that at the highest salt concentration (4.2 M) there is a non-negligible probability of the Li-F(FSI^-) coordination and aggregate formation that are essential for the LiF formation as a result of LiFSI reduction DME-LiFSI that are absent at low salt concentrations [13].

Further details of the evolution of the Li^+ coordination shell composition were obtained by examining the distributions of DME and FSI^- in it as shown in Fig. 7. We consider a DME or FSI^- anion to be coordinated by Li^+ if any of its oxygens were within 3.4 Å of a Li^+ cation. Examination of the probability of finding 0, 1, 2, 3 or 4 FSI^- anion complexed to the same Li^+ cation indicates that probabilities

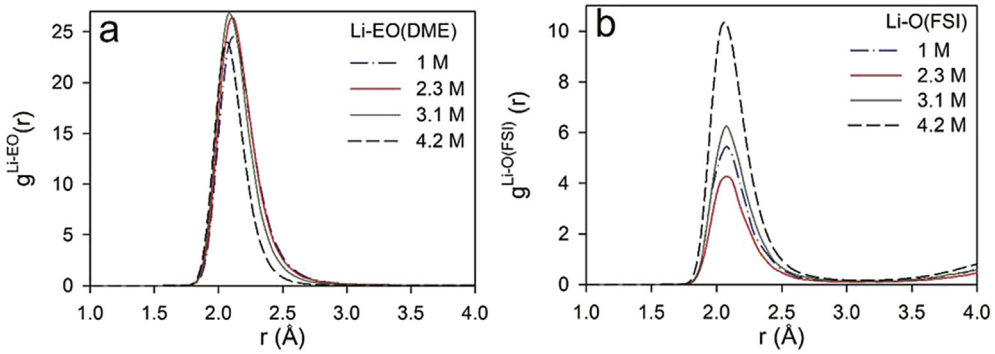

Fig. 5. Radial distribution functions for Li^+ with DME ether oxygen (a) and with oxygen of FSI^- (b).

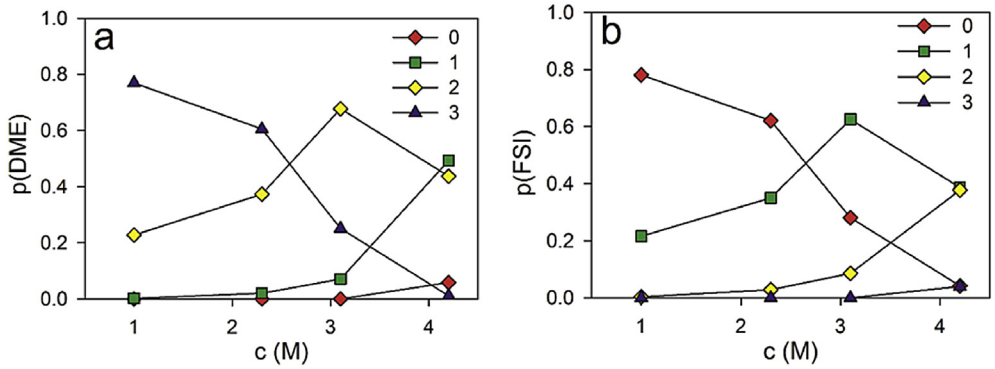

Fig. 7. Probability of finding a given number of DME solvents (a) and FSI^- anions (b) in the Li^+ first coordination shell.

are rather similar 1 M and 2.3 M electrolytes and changes dramatically between 2.3 and 4.2 M. At low salt concentrations below 2.3 M most Li^+ are not coordinated by FSI^- and a Li^+ cation has less than 35% probability to be coordinated by the FSI^- anion. At high salt concentration (4.2 M) 57% of Li^+ are coordinated by two or more FSI^- anions. On the other hand, most (96–99%) of DME coordinated Li^+ by both Oe with only a few percent of DME coordinated Li^+ via one Oe. The majority of FSI^- (71–75%) coordinated Li^+ with only one oxygen (not shown). Fig. 7 shows that at low salt concentration most Li^+ are coordinated by 3 DME molecules in accord with the crystal structures discussed above with a minor fraction of the Li^+ cation coordinated by 2 DME and one FSI^- anion. The fractions of the Li^+ cations that are coordinated by 3 DME with no FSI^- and by 2 DME with 1 FSI^- correspond reasonably well with the areas from fits to NMR data shown in Fig. 1b3 (also see Scheme 2 of 1 M concentration). At 3.2 M LiFSI concentration, there are three Li^+ environments present: Li^+(2DME + 1FSI^-), Li^+(3DME + 0FSI^-) with a minor contribution from Li^+(1DME + 2FSI^-), which consist with the gradual decrease of $Li^+(DME)_3$ and increase of $LiFSI(DME)_2$ discussed in Section 3.2.3. Therefore, the Li^+ coordination at this composition is the most heterogeneous. We tentatively attribute this heterogeneity in the Li^+ environments to the one of the largest widths of the Li^+ peak observed in NMR experiments at 3 M LiFSI in Fig. 1b5 (also see Scheme 2 of 3 M concentration). At the highest simulated salt concentration, the most probable observed Li^+ compositions are Li^+(1FSI^- + 2DME) and Li^+(2FSI^- + 1DME) with approximately equal contributions from each one, which agree with the quantum chemistry calculation results of $LiFSI(DME)_2$ (see Table 3 and Fig. 4b/c) and $Li^+(FSI^-)_2$DME (see Table 3 and Fig. 4m/n). At this salt concentration there is only a small fraction (4–6%) of Li^+ that are coordinated only by 4 FSI^- anions (not shown in Fig. 7) and no DME and most (95%) of the Li^+ cation are coordinated by at least one anion, thus the Li^+ environment at 4.2 M is less heterogeneous than that at 3.2 M corresponding. It corresponds well to the narrower peak for 4 M compared to 3 M observed in NMR experiments in Fig. 1b.

5. Conclusion

Natural abundance ^{17}O, ^6Li NMR and computational modeling of ^{17}O and ^6Li NMR chemical shifts are reported for the study of the solvation structures of LiFSI/DME electrolytes at various concentration of LiFSI. The use of ultra-high magnetic field and a large sample volume probe makes the acquisition of ^{17}O and ^6Li NMR spectra of various concentrations of LiFSI electrolytes with reasonable signal to noise ratio possible in an affordable experimental time. It was found that the chemical shifts of both ^{17}O and ^6Li changed with the concentration of LiFSI. The Oe ^{17}O chemical shifts associated with DME monotonically decreased with increasing LiFSI concentration. In dilute concentrations (<1 M) majority of solvates exist as $Li^+(DME)_3$ with a minor contribution from $LiFSI(DME)_2$. As LiFSI salt concentration increases beyond 2 M the LiFSI(DME) becomes the dominant solvate. Further salt concentration increase to 4 M gives rise to substantial population of $Li^+(FSI^-)_2$DME solvates. The DFT calculated ^{17}O and ^6Li chemical shifts on the composite solvation structures match well with the experimental results. In particular, the solvation structures associated with $Li^+(FSI^-)_2(DME)$ were key structures for matching DFT and NMR data. Furthermore, the Li^+ solvation structures predicted from MD simulation agreed well with the interpretation of NMR results using DFT calculated chemical shifts and further supported the NMR-based picture of the evolution of the Li^+ solvation.

Acknowledgment

This work was supported as part of the Joint Center for Energy Storage Research (JCESR), an Energy Innovation Hub funded by the U.S. Department of Energy, Office of Science, Basic Energy Sciences (BES). The NMR sample preparations were supported by the funding from the U.S. Department of Energy's (DOE's) Office of Electricity Delivery and Energy Reliability (OE) (under Contract No. 57558). The NMR, and computational studies were conducted in the William R. Wiley Environmental Molecular Sciences Laboratory (EMSL), a national scientific user facility sponsored by DOE's Office of Biological and Environmental Research (BER) and located at PNNL. PNNL is operated by Battelle for the Department of Energy under Contract DE-AC05-76RLO1830.

Appendix A. Supplementary data

Supplementary data related to this article can be found at http://dx.doi.org/10.1016/j.jpowsour.2015.12.120.

References

[1] M.S. Whittingham, Proc. Ieee 100 (2012) 1518–1534.
[2] W. Xu, J.L. Wang, F. Ding, X.L. Chen, E. Nasybutin, Y.H. Zhang, J.G. Zhang, Energy Environ. Sci. 7 (2014) 513–537.
[3] D. Aurbach, E. Zinigrad, Y. Cohen, H. Teller, Solid State Ion. 148 (2002) 405–416.
[4] F. Ding, W. Xu, G.L. Graff, J. Zhang, M.L. Sushko, X. Chen, Y. Shao, M.H. Engelhard, Z. Nie, J. Xiao, X. Liu, P.V. Sushko, J. Liu, J.G. Zhang, J. Am. Chem. Soc. 135 (2013) 4450–4456.
[5] D. Lu, Y. Shao, T. Lozano, W.D. Bennett, G.L. Graff, B. Polzin, J. Zhang, M.H. Engelhard, N.T. Saenz, W.A. Henderson, P. Bhattacharya, J. Liu, J. Xiao, Adv. Energy Mater. 5 (2015) 1400993.
[6] X. Bogle, R. Vazquez, S. Greenbaum, A.V.W. Cresce, K. Xu, J. Phys. Chem. Lett. 4 (2013) 1664–1668.

[7] K. Yoshida, M. Nakamura, Y. Kazue, N. Tachikawa, S. Tsuzuki, S. Seki, K. Dokko, M. Watanabe, J. Am. Chem. Soc. 133 (2011) 13121–13129.
[8] A. Plewa-Marczewska, M. Kalita, M. Marczewski, M. Siekierski, Electrochim. Acta 55 (2010) 1389–1395.
[9] B.D. McCloskey, D.S. Bethune, R.M. Shelby, G. Girishkumar, A.C. Luntz, J. Phys. Chem. Lett. 2 (2011) 1161–1166.
[10] O. Borodin, G.D. Smith, R. Douglas, J. Phys. Chem. B 107 (2003) 6824–6837.
[11] D. Aurbach, E. Granot, Electrochim. Acta 42 (1997) 697–718.
[12] Y. Lu, Z. Tu, L.A. Archer, Nat. Mater. 13 (2014) 961–969.
[13] H. Kim, F.X. Wu, J.T. Lee, N. Nitta, H.T. Lin, M. Oschatz, W.I. Cho, S. Kaskel, O. Borodin, G. Yushin, Adv. Energy Mater. 5 (2015) 1401792.
[14] Y. Yamada, M. Yaegashi, T. Abe, A. Yamada, Chem. Commun. Camb. 49 (2013) 11194–11196.
[15] Y. Yamada, K. Furukawa, K. Sodeyama, K. Kikuchi, M. Yaegashi, Y. Tateyama, A. Yamada, J. Am. Chem. Soc. 136 (2014) 5039–5046.
[16] Y. Yamada, K. Usui, C.H. Chiang, K. Kikuchi, K. Furukawa, A. Yamada, ACS Appl. Mater. Interfaces 6 (2014) 10892–10899.
[17] J. Qian, W.A. Henderson, W. Xu, P. Bhattacharya, M. Engelhard, O. Borodin, J.G. Zhang, Nat. Commun. 6 (2015) 6362.
[18] K. Matsubara, R. Kaneuchi, N. Maekita, J. Chem. Soc. Faraday Trans. 94 (1998) 3601–3605.
[19] O. Borodin, R. Douglas, G.D. Smith, F. Trouw, S. Petrucci, J. Phys. Chem. B 107 (2003) 6813–6823.
[20] L. Yang, A. Xiao, B.L. Lucht, J. Mol. Liq. 154 (2010) 131–133.
[21] M. Leskes, A.J. Moore, G.R. Goward, C.P. Grey, J. Phys. Chem. C 117 (2013) 26929–26939.
[22] E. Salager, V. Sarou-Kanian, M. Sathiya, M. Tang, J.-B. Leriche, P. Melin, Z. Wang, H. Vezin, C. Bessada, M. Deschamps, J.-M. Tarascon, Chem. Mater. 26 (2014) 7009–7019.
[23] J. Thielen, C.F. Kins, M. Schonhoff, H.W. Spiess, Appl. Magn. Reson. 45 (2014) 1063–1073.
[24] X. Deng, M.Y. Hu, X. Wei, W. Wang, Z. Chen, J. Liu, J.Z. Hu, J. Power Sources 285 (2015) 146–155.
[25] K. Hayashi, Y. Nemoto, S.-I. Tobishima, Y. Sakurai, J. Power Sources 81–82 (1999) 782–785.
[26] S. Grimme, J. Antony, T. Schwabe, C. Muck-Lichtenfeld, Org. Biomol. Chem. 5 (2007) 741–758.
[27] E. Van Lenthe, E.J. Baerends, J. Comput. Chem. 24 (2003) 1142–1156.
[28] O. Borodin, J. Phys. Chem. B 113 (2009) 11463–11478.
[29] O. Borodin, W. Gorecki, G.D. Smith, M. Armand, J. Phys. Chem. B 114 (2010) 6786–6798.
[30] S.D. Han, O. Borodin, D.M. Seo, Z.B. Zhou, W.A. Henderson, J. Electrochem. Soc. 161 (2014) A2042–A2053.
[31] S.B. Rempe, L.R. Pratt, G. Hummer, J.D. Kress, R.L. Martin, A. Redondo, J. Am. Chem. Soc. 122 (2000) 966–967.
[32] W.A. Henderson, J. Phys. Chem. B 110 (2006) 13177–13183.
[33] K. Izutsu, Electrochemistry in Non-aqueous Solutions, Wiley-VCH, Weinheim, Germany, 2009.
[34] O. Borodin, G.D. Smith, J. Solut. Chem. 36 (2007) 803–813.
[35] As discussed in Section 3.2.3., the Li^+ ion is fully solvated in $Li^+(DME)_3(DME)_8$ cluster.